



HAL
open science

Separation of poroelastic and elastic processes of an aquifer from tectonic phenomena using geodetic, seismic, and meteorological data in the Pollino region, Italy

Andrés Barajas, Piero Poli, Nicola d'Agostino, Ludovic Margerin, Michel Campillo

► To cite this version:

Andrés Barajas, Piero Poli, Nicola d'Agostino, Ludovic Margerin, Michel Campillo. Separation of poroelastic and elastic processes of an aquifer from tectonic phenomena using geodetic, seismic, and meteorological data in the Pollino region, Italy. *Geochemistry, Geophysics, Geosystems*, 2021, 10.1029/2021GC009742 . hal-03429180

HAL Id: hal-03429180

<https://hal.science/hal-03429180v1>

Submitted on 15 Nov 2021

HAL is a multi-disciplinary open access archive for the deposit and dissemination of scientific research documents, whether they are published or not. The documents may come from teaching and research institutions in France or abroad, or from public or private research centers.

L'archive ouverte pluridisciplinaire **HAL**, est destinée au dépôt et à la diffusion de documents scientifiques de niveau recherche, publiés ou non, émanant des établissements d'enseignement et de recherche français ou étrangers, des laboratoires publics ou privés.

1 **Separation of poroelastic and elastic processes of an**
2 **aquifer from tectonic phenomena using geodetic,**
3 **seismic, and meteorological data in the Pollino region,**
4 **Italy**

5 **Andrés Barajas¹, Piero Poli¹, Nicola D'Agostino², Ludovic Margerin³, Michel**
6 **Campillo¹**

7 ¹ISTerre
8 ²INGV
9 ³IRAP

10 **Key Points:**

- 11 • Noise-based velocity variation measurements are explained by modeled water lev-
12 els inside an aquifer
13 • Geodetic evidence of elastic and poroelastic response of the zone to the rainfall
14 • Identification of the effect of seismic active period in the velocity variations

Corresponding author: Andrés Barajas, custore@gmail.com

Abstract

Velocity variations obtained from ambient seismic noise are sensitive to many factors. We aimed to disentangle these processes in a 10-year-long recording of seismic noise from a single station in the Pollino region, in southern Italy. This region is characterized by aquifers and by a relatively short period of high seismic activity that included slow slip events and a M_W 5.0 earthquake that occurred on October 25, 2012. We apply two models that estimate the water level inside an aquifer, which show a good correlation with the measured $\delta v/v$, showing that the velocity variations are inversely proportional to the pore pressure inside the aquifer. Our interpretation is further confirmed by geodetic measurements that show that in a direction parallel to the strike angle of the fault rupture, the expansion-contraction displacement of the zone follows the same patterns observed in the models and in the velocity variations, as a result of the pressure generated by the water on its interior. Going one step further, we analyze the nature of the small discrepancies between the measured and modeled velocity variations. These correlate well with the rainfall and with the vertical geodetic measures, which indicates an elastic response of the zone to the loading generated by the rainwater. Comparisons between these variables allow us to clearly identify the period of the seismic activity in the zone, which is represented by the characteristic drop in the seismic velocity in the period from the beginning of 2012 to mid-2013.

1 Introduction

Analysis of ambient seismic noise (Campillo & Paul, 2003; Shapiro & Campillo, 2004; Campillo, 2006) has allowed estimation of changes in the velocities in the crust related to a variety of phenomena, such as earthquakes (Breguier, Campillo, et al., 2008), volcanic activity (Rivet et al., 2015; Breguier, Shapiro, et al., 2008), and the thermoelastic responses of the soil (Meier et al., 2010), among others. Many studies have focused on the hydrological effects on the $\delta v/v$. Sens-Schönfelder and Wegler (2006) estimated the underground water levels using a model developed by Akasaka and Nakanishi (2000), to define the direct relations to the measured velocity variations in a volcano. Meier et al. (2010) analyzed velocity variations within the Los Angeles basin (USA), and concluded that the seasonal variations are strongly influenced by groundwater level changes and thermo-elastic strain variations. Clements and Denolle (2018) found a direct correlation between velocity variations measured through seismic noise and measurements of the groundwater level. Tsai (2011) proposed periodic models to recreate displacement and velocity changes from thermo-elastic stress and hydrological loading. Wang et al. (2017) reported a direct relation between velocity variations and several hydrological and meteorological processes across Japan, which were mainly based on the pore pressure generated by rainwater through a diffusion process. Hillers et al. (2014) showed a correlation between velocity changes and periodicity of precipitation events in Taiwan.

Hydrological deformation processes have also been studied through geodetic data (Bawden et al., 2001; Watson et al., 2002; Borsa et al., 2014; Chanard et al., 2014). In general, the effects of rainfall can be seen in two ways: as an elastic response where the water exerts a loading pressure that subsides the surface (Amos et al., 2014; Argus et al., 2014; Nof et al., 2012); or as a poroelastic response that generates a rise in the surface as a consequence of the recharging of the porous inner structure of the soil (Galloway & Burbey, 2011; King et al., 2007).

From the aforementioned studies, it emerges that the thermal and hydrological effects on $\delta v/v$ are significant, and these can thus mask velocity changes induced by tectonic processes. It is therefore fundamental to quantify such environmental effects, to resolve the velocity variations induced by tectonic processes in studies of the physics of faults. Examples of this approach include the study of Hillers et al. (2019), where seasonal variations were filtered out, to highlight deformation patterns of tectonic origin around

66 the San Jacinto fault (USA), and the study of Poli et al. (2020), where tectonic and hydro-
 67 logical processes were separated from a single station analysis of $\delta v/v$. In the present
 68 study, we pursue this same objective: we disentangle the influence of the water content
 69 inside the crust from the tectonic events.

70 One of the main characteristics of this zone is the presence of karst aquifers, which
 71 are likely to be the driving factor behind the non-steady, transient behavior found in seismic
 72 velocity measurements and geodetic displacements (Poli et al., 2020; D’Agostino et
 73 al., 2018). The highest precipitation of the zone usually happens between November and
 74 February, with low to moderate rainfall in the summer. In this region is present the mas-
 75 sif Pollino where temperatures can greatly vary depending on the altitude that can be
 76 up to 2267 *m*. This area was relatively inactive seismically until the beginning of 2012,
 77 when a seismic swarm began that lasted until the middle of 2013, a period that included
 78 several earthquakes, such as a M_W 5.0 event on October 25, 2012 (Passarelli et al., 2015).
 79 It has been estimated that 75 percent of 6000 events detected during the swarms were
 80 not aftershocks, which means that the driving mechanism behind the swarm might be
 81 a transient forcing. The physical nature of this transient forcing might be fluid filtration,
 82 pore pressure diffusion, or aseismic slow slip (Parotidis et al., 2003; Peng & Gombert,
 83 2010). This last scenario can also be associated with fluid-related phenomena that can
 84 reduce the normal stress in the fault. It has also been suggested that a large part of the
 85 crustal deformation in the zone arises through transient slow slip events (Cheloni et al.,
 86 2017).

87 In this study, we measure the seismic velocity variation $\delta v/v$ in the Pollino region,
 88 Italy (Figure 1), from ambient seismic noise recorded by a single station over nine years.
 89 We determine the role of the water in the $\delta v/v$ measurements by comparing them with
 90 two different models that calculate the water levels inside an aquifer based on record-
 91 ings of the rainfall. Based on these models, the contribution of the water inside the aquifer
 92 to the $\delta v/v$ is estimated. The interpretation of the mechanism through which the wa-
 93 ter in the aquifer controls the velocity variations is consistent with independent horizon-
 94 tal geodetic measurements that show an expansion-contraction behavior of the region
 95 with the same characteristics of the seismic measurements and the modeled water con-
 96 tents in the aquifer. Afterward, the modeled velocity variation produced by the stored
 97 water in the aquifer is removed from the seismic measurements, allowing the analysis of
 98 other phenomena that are also present in seismic records. A weaker pattern is identi-
 99 fied, mainly controlled by the immediate elastic response of the zone to the rainfall, which
 100 is also the main driving factor behind the variations in the vertical geodetic measure-
 101 ments. Finally, this procedure reveals a velocity drop that is most probably related to
 102 the stress release of the zone through seismic activity.

103 2 Data processing

104 The overall layout of the data-collection stations is shown in Figure 1. The seis-
 105 mic ambient noise was recorded at station MMNO in the Pollino area (Italy) (INGV Seis-
 106 mological Data Centre, 2006). The three-component continuous signals are band-passed
 107 between 0.5*Hz* and 1.0*Hz*. For each day, the whole signal is divided into overlapping
 108 windows of 30 min each (50% overlap). We then calculate the cross-correlation between
 109 the 30-min windows for all the possible combinations of the three available channels. This
 110 means that for each 30-min segment, we obtain six cross-correlations. In practice, we cal-
 111 culate these simultaneously using the Covnet package (Seydoux et al., 2017). The 30-
 112 min cross-correlations are averaged for each day, which results in six cross-correlations
 113 per day. Afterward, to stabilize the signals obtained and to reduce possible transient noise
 114 sources, the correlations are replaced by the moving average of correlations within a win-
 115 dows of 30 days around each day. Finally, six global reference cross-correlations are ob-
 116 tained by averaging all the available correlations. Variations in the velocity can be es-
 117 timated if we consider that a perturbation in the medium will generate a change in the

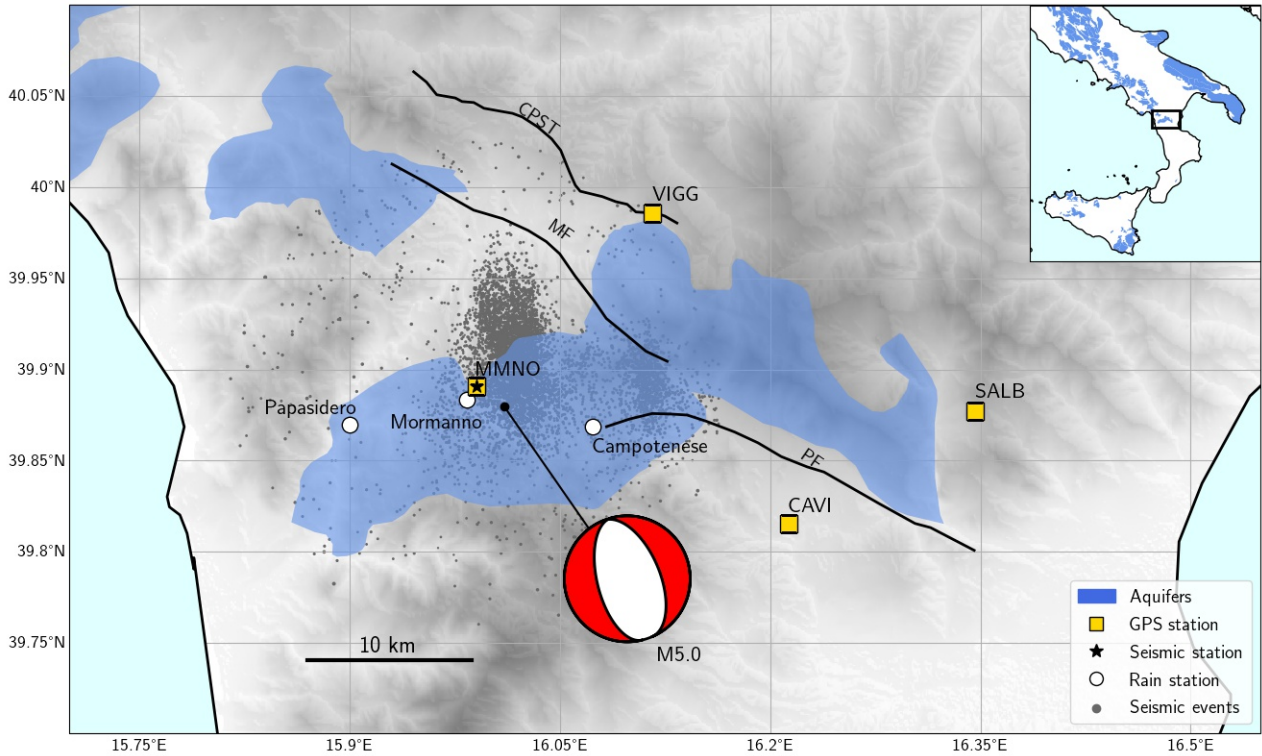


Figure 1. General disposition of the seismic, rain and GPS stations, and location of the aquifers and the $M_W 5.0$ earthquake, in the study area in Calabria, Italy. The CPST, MF and PF lines represent the Castello Seluci-Timpa della Manca, Mercure, and Pollino faults, respectively (Michetti et al., 2000; Papanikolaou & Roberts, 2007). The rain data was obtained from the Multi-risk Functional Centre (ARPACAL, n.d.).

118 shape of the daily cross-correlation with respect to the global average, in the same way
 119 that a pulse emitted in the position of the seismic station would be registered differently
 120 if the velocity of the medium change. We calculate this possible change with the Mov-
 121 ing Window Cross Spectral analysis (Poupinet et al., 1984) using the segment of the coda
 122 of the cross-correlations between 10s and 50s. We assume that the phenomena we want
 123 to observe do not depend on the direction of the seismic field and therefore, the six dif-
 124 ferent combinations are averaged between them daily to decrease the level of noise in the
 125 measurements. Finally, a moving average of 30 days is applied over the resulting $\delta v/v$
 126 series.

127 The GPS displacements were obtained from rinex data of GNSS stations belong-
 128 ing to the Rete Integrata Nazionale GPS network (Istituto Nazionale di Geofisica e Vul-
 129 canologia INGV, 2016). These data were processed using the Jet Propulsion Laboratory
 130 GIPSY-OASIS II software following the procedure used in D'Agostino et al. (2018).

131 The rain data were collected from the three closest stations available, as shown in
 132 Figure 1. Data were not available for all the study period from all the three stations, so
 133 an averaging process was carried out for each day using the available information for that
 134 day. This provides an estimation of the regional daily rainfall, which is shown in Fig-
 135 ure 2a.

136 Figure 2b shows the accumulated seismic moment per day in a radius of 15km around
 137 the station MMNO, and the slip-rate reported by Cheloni et al. (2017). The aseismic
 138 slip rate is estimated from a time dependent inversion over GPS observations and line-
 139 of-sight displacements derived from short repeat-time Synthetic Aperture Radar images,
 140 assuming a uniform slip on the rupture plane. The data is inverted to obtain the dimen-
 141 sions, positions and strike, dip and rake of the fault plane. The results of the inversion
 142 showed that the main area of transient aseismic slip took place between 2km and 7km
 143 along a source model that is consistent with the coseismic fault plane of the $M_W 5.0$ event
 144 on October 25, 2012 mainshock.

145 3 Procedure and results

146 3.1 Measured and modeled velocity variations

147 The noise-based velocity variations shown in Figure 2a reveal several patterns. There
 148 is a periodic (1 year) oscillation that appears to be related to the amount of water in
 149 the crust (*i.e.*, the regional daily rainfall). Indeed, the daily rain observed on the region
 150 (Fig. 2a) increases during the winter, which appears to be associated with velocity re-
 151 ductions (Sens-Schönfelder & Wegler, 2006). Beyond the periodic signal, a long-term trend
 152 of increasing velocity is observed over the full study after 2014 (Fig. 2a).

153 To separate the hydrological signals from the effects of possible changes in tectonic
 154 stress in the seismic $\delta v/v$ series, the induced velocity variations generated by the water
 155 in the crust are modeled. For this, we developed and applied two different models that
 156 estimate the accumulated water inside the aquifer as a function of time.

157 The aquifer is recharged by the rainfall through a rapid process that is due to the
 158 characteristic permeable material of the karst. We assume that this happens at a higher
 159 velocity than for normal diffusion processes: the rainfall is added each day directly to
 160 the water level of the aquifer. The discharge process can be described by two different
 161 models, both of which are related to the stored water inside the aquifer.

162 The first model, as a linear reservoir (Fiorillo, 2011), assumes that the aquifer loses
 163 water through flux with its surroundings at a discharge rate dQ/dt (where Q is the stored
 164 volume of water) that is proportional to the difference in the amount of water between
 165 the interior and the exterior of the karst $\Delta\phi$, and the contact area between the two A_L

$$\frac{dQ}{dt} = U A_L \Delta\phi + R \quad (1)$$

166 where R is any external source supplying the aquifer, and U has the role of a con-
 167 ductance over the surface, *i.e.*, the proportionality constant between the flux of water
 168 leaving the aquifer (per unit area) and the difference in the amounts of water; indeed,
 169 U is the equivalent of the heat transfer coefficient in the heat transfer Newton's law of
 170 cooling. From this point of view, this parallels the obtaining of Newton's law of cooling
 171 from the heat equation, which is also defined as a diffusive process. The total amount
 172 of water inside the aquifer can be defined in terms of its density and the volume it oc-
 173 cupies. The water in the aquifer accumulates at its bottom, and therefore, this volume
 174 can be defined in terms of the area of the bottom A_B and the height of the column of
 175 water h . On the other hand, we assume that the area that transmits water is just the
 176 lateral one (with no difference in the amount of water flux at the top or the bottom).
 177 Then, the contact area can be defined as approximately the product of the perimeter P
 178 and the height of the column of water $A_L = P * h$. Introducing these changes into the
 179 discharge equation turns it into

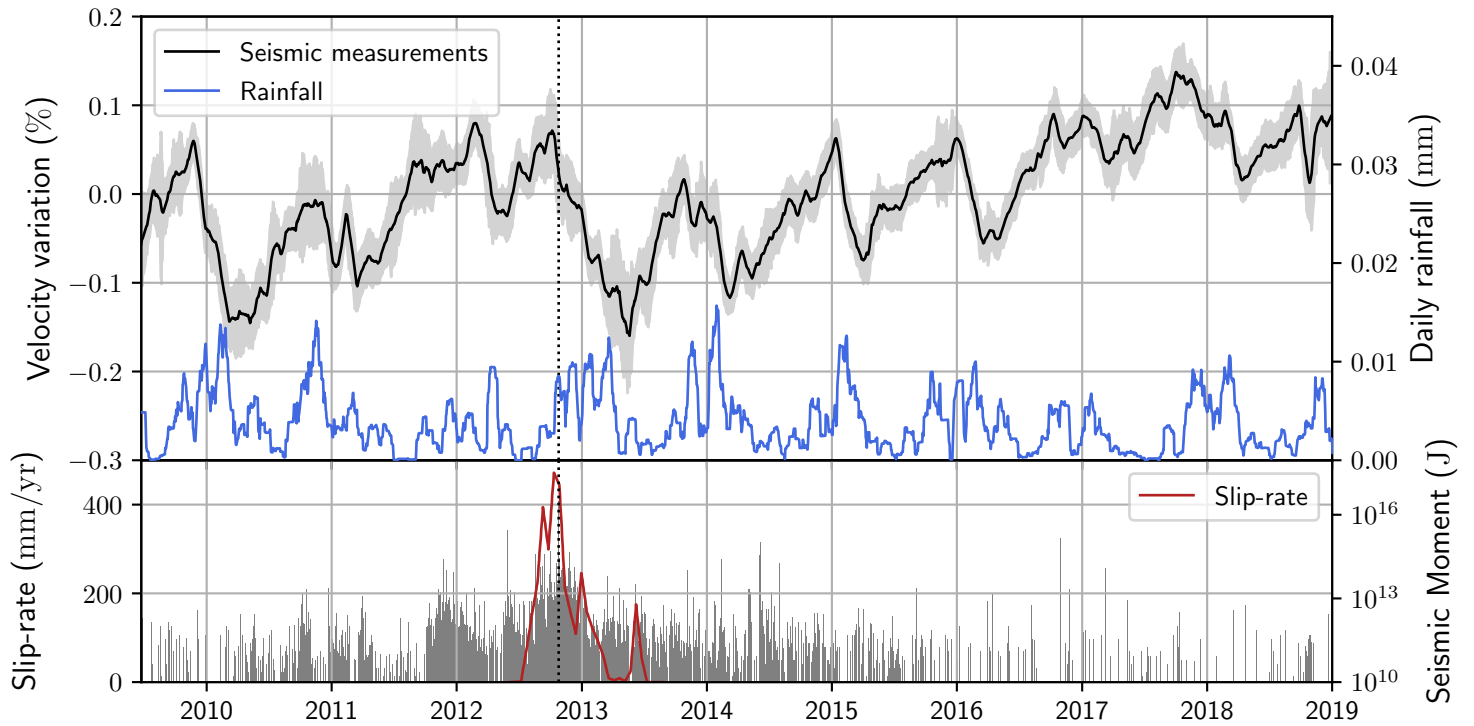


Figure 2. (a) Seismic measurements of $\delta v/v$ and the moving average of the daily rainfall in the region calculated over a window of 30 days. The gray area represents the measurements error calculated by the Moving Window Cross Spectral analysis. (b) Daily accumulated seismic moment in the region, and slip-rate as reported by Cheloni et al. (2017). The dashed line indicates the date of the $M_W 5.0$ seismic event.

$$\frac{d(A_B h)}{dt} = UP h \Delta \phi + R \quad (2)$$

180 which means that the rate at which the aquifer loses water is proportional to the
181 water level itself

$$\frac{dh(t)}{dt} = -kh(t) + r \quad (3)$$

182 where h is the water level inside the aquifer, r is the source term defined in terms
183 of the change it generates in the water level inside the aquifer, and $k = UP\Delta\phi/A_B$,
184 which depends on the geometry of the aquifer and the conductance of the medium.

185 The second model, as the Torricelli reservoir (Fiorillo, 2011), assumes that the aquifer
186 works as a container that loses water through spring-loading at its bottom. The veloc-
187 ity at which the water leaves the aquifer is proportional to the square root of the height
188 of the water it contains, as stated by Torricelli's law

$$v = \sqrt{2gh} \quad (4)$$

189 where g is gravity. In this case, the discharge can be defined in terms of this ve-
190 locity and the area through which the water escapes (A_s)

$$\frac{dQ}{dt} = A_s v + R = A_s \sqrt{2gh} + R \quad (5)$$

191 If we define the volume of water inside the aquifer again as $A_B h$, the change in the
192 water level will follow the same mathematical structure

$$\frac{dh(t)}{dt} = -k' \sqrt{h(t)} + r \quad (6)$$

193 where $k' = A_s \sqrt{2g}/A_B$, and r is the source that supplies the aquifer in terms of
194 the water level. The constants in both of these equations are related to the physical char-
195 acteristics of the aquifer, and modifying them changes the strength and the delay of the
196 discharge for a given amount of water inside the aquifer.

197 Therefore, the water level each day will be the level of the day before, plus the level
198 gained by the rainfall on that day r , minus the losses that are calculated according to
199 the model:

$$h_{i+1} = h_i - kf(h_i) + r_i \quad (7)$$

200 Here, $f(h_i)$ is the particular functional dependence of the model on the water level,
201 as defined by Equations 3 or 6. It must be noted that none of the two models take into
202 account other possible factors that may increase or decrease the total amount of water
203 in the aquifer, like evapotranspiration.

204 The units of the water level obtained by the models are the same as the units of
205 the rainfall, which is measured as *mm* water recollected per square meter. This means
206 that recollected the totality of the indicated rainfall (which is most probably not the
207 case), will produce the water levels estimated by the models only if we have an aquifer
208 of exactly $1m^2$. Furthermore, if the area that collects the water (*i.e.*, the area of the aquifer)
209 is different from the area that supplies the rainwater, the proportionality between these

210 two units will not be 1-to-1. This implies that both models allow us to estimate relative
 211 changes in the water level, but not its absolute value. However, this is not a problem,
 212 as will become clear below.

213 If the water level controls the velocity variation, the resulting series for h should
 214 show the same behavior as $\delta v/v$; or in other words, they will have a linear relationship.
 215 The value of the constant k in each model that optimizes the linear relation between these
 216 can be defined through the following grid search:

- 217 1. A value of k is chosen, and using the rain data as the input, the water level time
 218 series is calculated following the recursive formula of Equation 7
- 219 2. The water level is shifted towards zero, which removes its time average (represented
 220 by $\langle \cdot \rangle$):

$$h(t) \rightarrow h(t) - \langle h(t) \rangle \quad (8)$$

- 221 3. The proportionality constant between $(\delta v/v)(t)$ and the water level time series is
 222 calculated as the ratio between the covariance and the variance: $a = \text{cov}((\delta v/v)(t), h(t)) / (\text{var}(h(t)))$
 223 (Rivet et al., 2015).
- 224 4. The shift or intercept between the two series is estimated as the average of the seis-
 225 mic velocity variation: $b = \langle (\delta v/v)(t) \rangle$
- 226 5. A synthetic velocity variation $\delta v/v_{syn}$ is obtained from the water level model us-
 227 ing both constants a and b :

$$\frac{\delta v}{v}_{syn}(t) = \left\langle \frac{\delta v}{v}(t) \right\rangle + \left(\frac{\text{cov}(\frac{\delta v}{v}(t), h(t))}{\text{var}(h(t))} \right) \cdot h(t) \quad (9)$$

- 228 6. For a given constant k , the fit to the data of the model to describe the seismic ve-
 229 locity variation is measured as

$$\sigma^2(k) = \frac{1}{n} \sum_{i=1}^n \left(\frac{\delta v}{v}(i) - \frac{\delta v}{v}_{syn}(i, k) \right)^2 \quad (10)$$

- 230 7. The process is repeated for a whole set of values of k , and the $\frac{\delta v}{v}_{syn}$ with the low-
 231 est σ^2 (the most similar to the measured $\frac{\delta v}{v}$) is chosen.

232 The models produce almost indistinguishable results because the daily input will
 233 only highlight any linear dependence in the long term. The misfit of each model and a
 234 comparison between them are given in the Supplementary Material. The synthetic ve-
 235 locity variation obtained with the linear reservoir model for the best-fit constant can be
 236 seen in Figure 3a; this will be the model used in the rest of this paper. In both cases,
 237 the covariance between the seismic measurements and the water level model is negative,
 238 which means that they are anti-correlated: an increase in the amount of water in the aquifer
 239 results in a decrease in the seismic velocity in the medium. This happens because the
 240 presence of water increases the pore pressure, which in turn reduces the overall effective
 241 pressure in the zone, and therefore reduces the seismic velocity. We can see that the mod-
 242 els accurately reproduce the seismic-based series, not only for its seasonal patterns, but
 243 also for the overall multi-year trend, which means that the water content in the aquifer
 244 is effectively the main driving factor behind the recorded velocity variations and that the
 245 water is being accumulated within the sensitivity range of the analyzed frequency of the
 246 seismic waves. The positive trend observed from 2014 to 2019 is a regional multi-annual
 247 hydrological trend that is also observed in the spring discharge and in the modulation
 248 of the seismicity along the Irpinia Fault (D'Agostino et al., 2018). The change in rela-
 249 tive amplitude and phase between the rain and the water level model is illustrated in the
 250 supplementary Figure S3.

251 The difference between the measured velocity changes and the modeled velocity
 252 changes can be seen in Figure 3b. There is a periodic misfit between these, which means

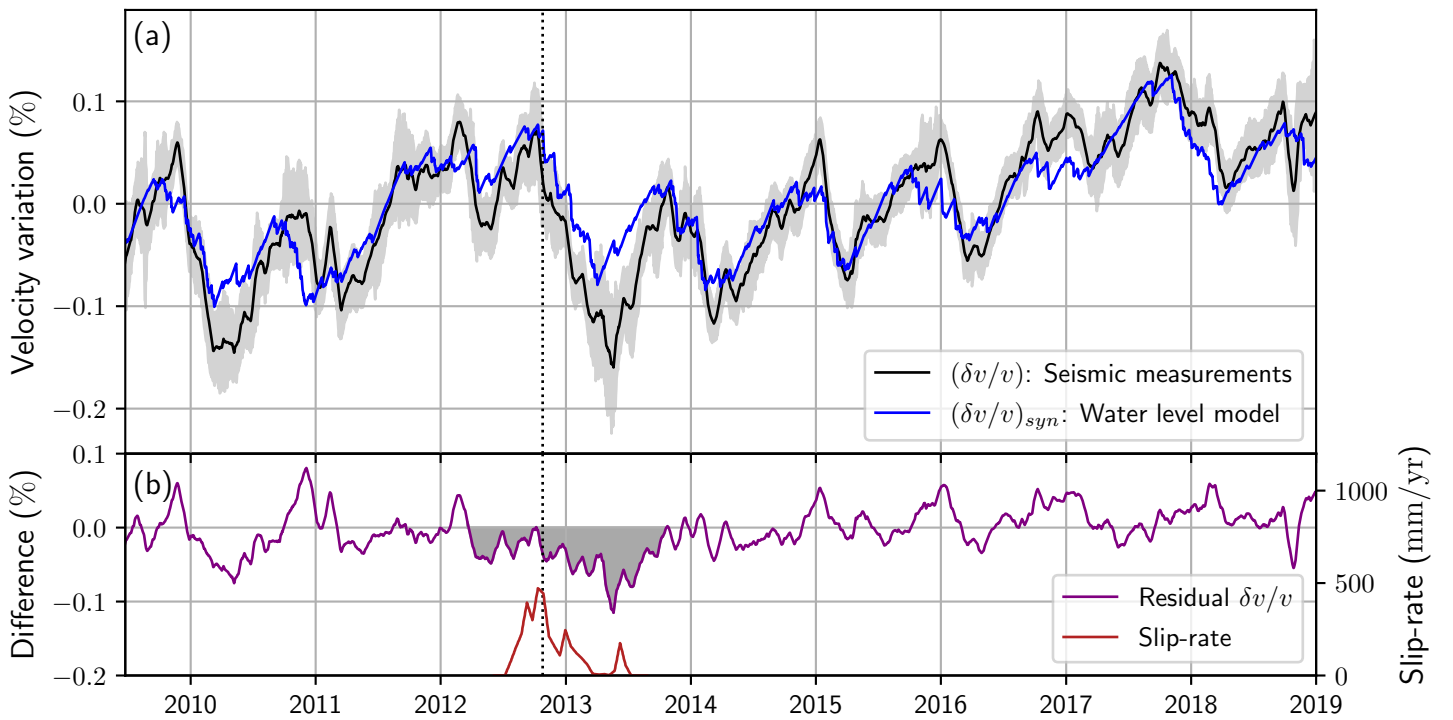


Figure 3. Seismic noise measurements and water level model. (a) Seismic and synthetic $\delta v/v$ obtained from the water level model. The gray area represents the measurements error calculated by the Moving Window Cross Spectral analysis. (b) Difference between the model and the measured $\delta v/v$ smoothed with a 30-day window and the reported slip-rate from Cheloni et al. (2017). The shaded zone highlights the systematic excess of velocity reduction between the seismic $\delta v/v$ and the rain-based model. The dashed line marks the date of the M_W 5.0 seismic event

253 that a small part of the seismic velocity variation is not explained by our models. This
 254 might be due to a defect in the model or to the presence of a second phenomenon that
 255 acts in parallel with the water accumulation. Furthermore, the most remarkable feature
 256 of this difference is a systematic excess of velocity reduction, which starts at the begin-
 257 ning of 2012, when there was high seismic activity, and lasts approximately until the end
 258 of 2014. Here, the velocity changes measured in the seismic field are not completely ac-
 259 counted for by the water level model, *i.e.*, by the accumulated water that can increase
 260 the hydraulic head and the aquifer pore pressure. Although the 30-day moving average
 261 applied over the time series makes it difficult to define specific dates, this systematic dif-
 262 ference appears to be generated by tectonic stress release, as it happens simultaneously
 263 with the seismic activity. Furthermore, through 2013, this difference appears to increase,
 264 having its maximum peak around the same time as the last pulse of the reported slow
 265 slip in the zone. It was shown that this late slip happened simultaneously with an en-
 266 largement of the crustal area affected by the seismicity (Cheloni et al., 2017). However,
 267 the systematic difference with our model extends for several months beyond the slow slip
 268 event. This extended behavior might be related to the stress change produced by the con-
 269 tinuous low intensity seismicity which may drop the velocity variation in the same way
 270 as registered by Brenguier, Campillo, et al. (2008) for big seismic events. It is also pos-
 271 sible that the earthquake or the slow slip changed the internal structure of the aquifer,
 272 which would produce a migration of water that might temporarily change the water level.
 273 Whatever the cause here, the changes in the velocity are completely recovered by the end
 274 of 2013.

275 3.2 Analysis of the geodetic data

276 Geodetic measurements are useful to measure displacements related to earthquakes
 277 and to slow slip events, and also to analyze hydrological processes inside aquifers (Cheloni
 278 et al., 2017; D’Agostino et al., 2018; Silverii et al., 2016).

279 We turned to an analysis of GPS traces as an independent way to assess the mod-
 280 eled variation of the velocity and its possible mechanisms. For this, we used GPS traces
 281 obtained from four stations in the study area, as shown in Figure 1.

282 The GPS displacements show trends produced by the movement of the underly-
 283 ing tectonic plate movement. One possibility to overcome this problem would be to de-
 284 trend each of the GPS displacements with the mean displacement calculated from a group
 285 of stations. However, different stations would result in different mean trends, which means
 286 that the final result would depend on the choice of stations to include in the analysis.
 287 We use the relative displacements between stations, as they are independent of the ref-
 288 erence frame and reflect only the deformation between the two stations.

289 We begin by analyzing the relative displacement between the two stations closest
 290 to the earthquake, VIGG and MMNO, with smoothing with the same 30-day window
 291 as for the velocity variation. Both of the relative horizontal components are shown in
 292 Figure 4a. To simplify the visualization of the GPS traces, they have all been shifted ver-
 293 tically towards zero without modifying their behavior or their relative values. This does
 294 not affect our analysis, as we are interested in the patterns described by the traces and
 295 not in their absolute values. The relative displacement shows seasonal patterns in all the
 296 directions and a clear change in the baseline due to the M_W 5.0 event.

297 Perhaps the most interesting feature of the traces in Figure 4a is the behavior of
 298 the NS component from 2014 until the end of the series, as it shows a similar pattern
 299 to that observed in the $\delta v/v$: a yearly seasonal variation over a multiyear increasing be-
 300 havior, with approximately the same shape. However, this behavior is not seen in the
 301 EW direction. There are two reasons why this behavior is not seen for both components.
 302 One of these is a possible anisotropic response of the aquifer to the hydrostatic pressure
 303 in the horizontal direction (Silverii et al., 2016). Commonly, a porous medium like an

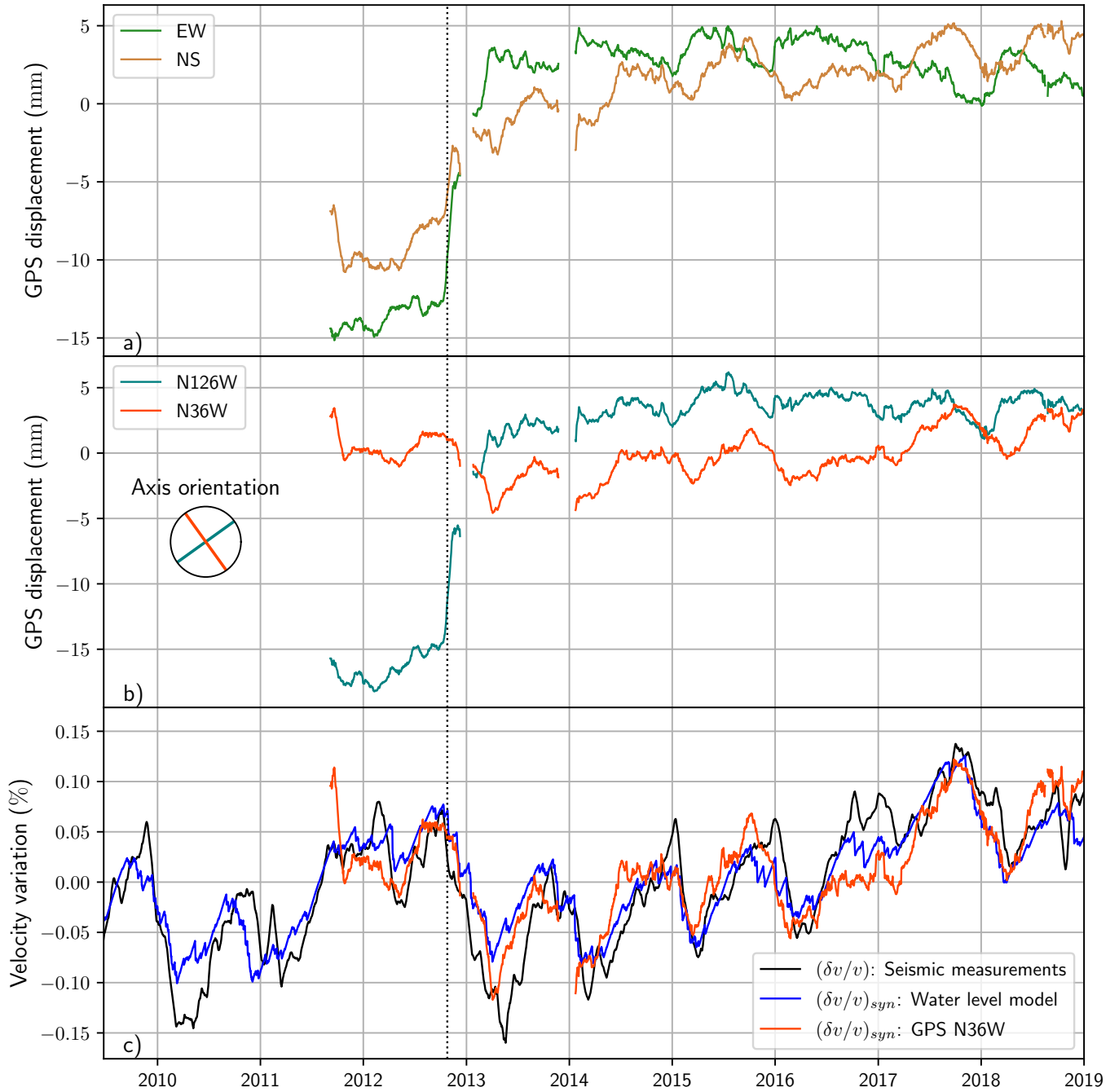


Figure 4. Modeled velocity variations and GPS relative displacements. (a) Relative horizontal GPS displacements between stations MMNO and VIGG. (b) GPS horizontal relative displacements rotated by an angle of 36° in a counterclockwise direction. (c) Velocity variations measured through seismic noise analysis, as estimated from the water level model, and fitted with the rotated $N36W$ horizontal displacement. The dashed line indicates the date of the $M_W 5.0$ seismic event.

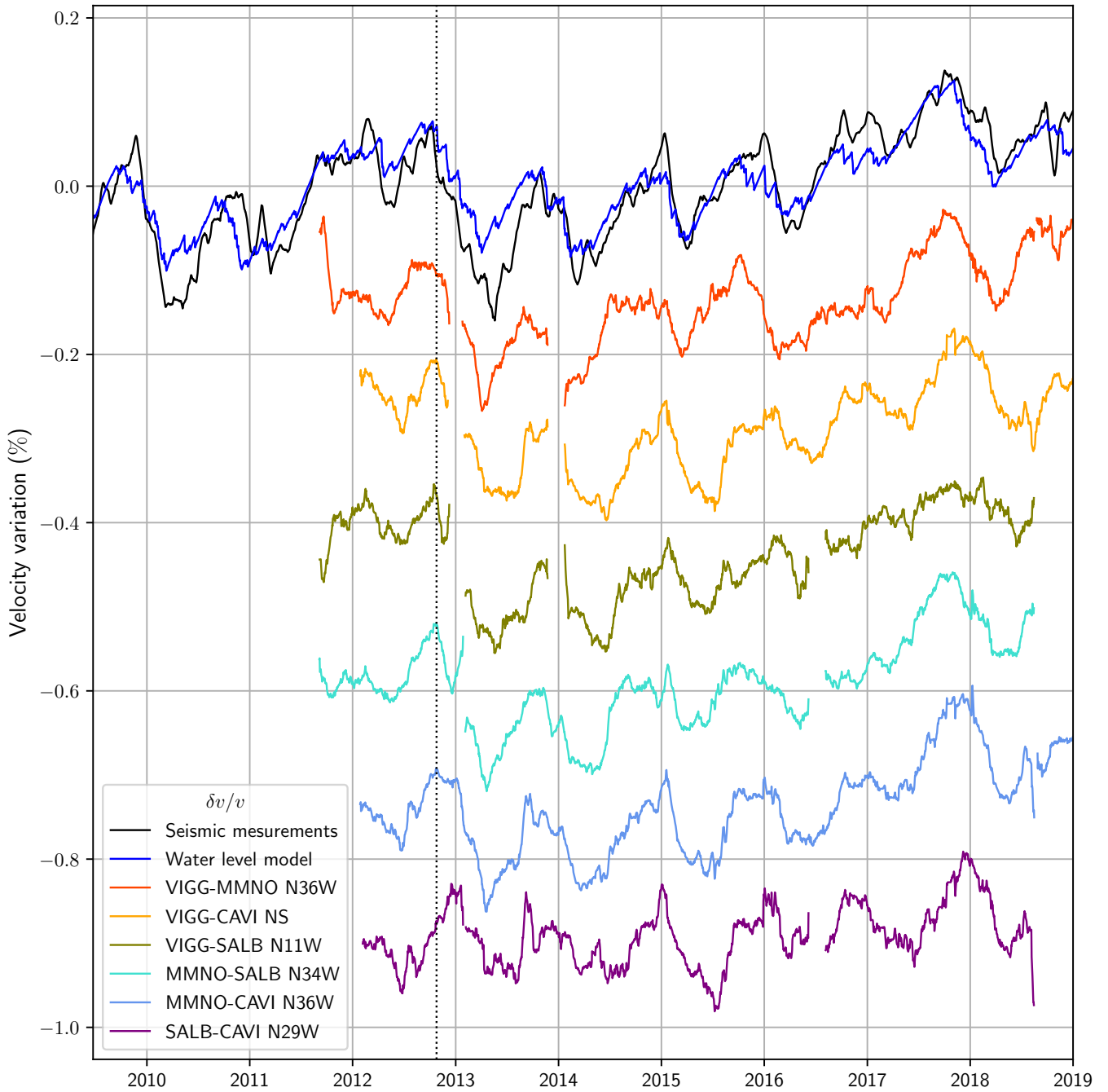


Figure 5. Comparisons between the measured velocity variations (black) and all the synthetic velocity variations obtained with the water level model (blue line) and with rotation of the GPS relative displacements for all the possible combinations between the four stations. A shift of 0.15% was introduced between these for clarity of presentation. The angle of the rotation that maximizes the fit for each couple is indicated in the key (bottom left), except for VIGG-CAVI, where no rotation was needed. The dashed line indicates the date of the $M_W 5.0$ seismic event.

304 aquifer has fractures that can open and close temporarily according to the pressure gen-
 305 erated by the water (Amoruso et al., 2014; Daniele et al., 2012). If these fractures lie pre-
 306 dominately in a specific direction, the macroscopic expansion-contraction dynamics will
 307 be more (or only) visible in this direction, which constitutes an anisotropic response. An-
 308 other possible reason might simply be the relative position of the GPS station to the aquifer:
 309 *e.g.*, if we had a GPS station at the north of a perfectly circular aquifer, we would ex-
 310 pect to see the expansion-contraction recorded only in the NS component and not in the
 311 EW component, even in an isotropic fracture system.

312 Most likely, the main expansion-contraction direction is not exactly NS. With this
 313 in mind, a rotation is performed for the horizontal GPS traces, to find the angle that max-
 314 imizes the presumed linear relation between the GPS displacement and the modeled water
 315 level inside the aquifer. This is done through a similar grid search between one ro-
 316 tated component of the GPS and the measured seismic $\delta v/v$, as described at the end of
 317 section 3.1.

318 Figure 4b shows the rotated GPS at the best fit angle. The reason why this an-
 319 gles minimizes the fit can be seen in Figure 4c: the trace in the direction N36W shows
 320 the same behavior as the modeled velocity variations for all times, even in the period in
 321 which the earthquake and the slow slip occurred. There are two reasons why this trace
 322 follows the water level in the aquifer so well. The first is that the direction of this ro-
 323 tated GPS is the only direction in which the fault rupture of the earthquake is not vis-
 324 ible; *i.e.*, the direction of the strike angle of the earthquake. This is important, as any
 325 other direction will show a discontinuity in the horizontal expansion of the aquifer. On
 326 the other hand, it is possible that the localization of the GPS station, which is NW of
 327 the aquifer, helps to accentuate the expansion-contraction process in that specific direc-
 328 tion.

329 Beyond the mechanism that accentuates one direction in particular, it is clear that
 330 the behavior of the displacements is related to the variations seen in both the velocity
 331 changes and in the water model, which is coherent with an expansion-contraction poroe-
 332 lastic dynamic in the aquifer (Amoruso et al., 2014; Chaussard et al., 2014; Ojha et al.,
 333 2019). As the aquifer stretches between the four GPS stations, this process should be
 334 visible using different combinations of the stations, and not only between VIGG and MMNO.
 335 In effect, calculation of the relative displacement between all the other paired stations,
 336 and finding of the best rotation for each case, produces a similar pattern, as can be seen
 337 in Figure 5. Although different GPS combinations fit better around different angles, all
 338 the combinations that involve station MMNO (the closest to the seismic event) are max-
 339 imized around 36 degrees, possibly as a consequence of finding the projection that does
 340 not show the effect of the earthquake itself. Moreover, it can be seen that different sta-
 341 tion pairs produce different levels of intensity between the seismic event and the water-
 342 driven pattern. This indicates a possible new way to analyze the complexity of the sys-
 343 tem, and particularly the directions of the volumetric expansion of the area.

344 4 Loading effect of the rainfall

345 A deeper inspection of the seismic velocity variations can be made if we analyze
 346 the part of it that is not controlled by the water level in the aquifer. This can be done
 347 by subtracting one from another, as is shown in Figure 6a. This is the same difference
 348 to that shown in Figure 3, but processed with a longer moving average window of 180
 349 days, calculated over each day, to stabilize the fluctuations and highlight the seasonal
 350 patterns. The longer smoothing window and the representation of the difference between
 351 the measured and modeled velocity variations explains why the amplitude of the pat-
 352 tern obtained is around 20 percent of the original amplitude of the velocity. As was seen
 353 in Figure 3, this residual velocity is not in phase with the modeled water level in the aquifer.
 354 However, a quick inspection of the rainfall smoothed over the same moving average win-

dow of 180 days (Figure 6b) reveals that both are in phase, which means that the observed behavior probably comes from the loading that the rainfall generates over the surface. This conclusion is confirmed by the vertical component of the GPS stations in the regions that show a negative correlation between the rainfall itself and the height of the surface (Figure 6c) (Amos et al., 2014; Argus et al., 2014; Nof et al., 2012). Although the three measurement series in Figures 3a 3b and 3c are in phase, their relative amplitudes are different, even between the two GPS vertical displacements. This is probably due to particularities of the local structure around each of the stations and to differences in the surface size to which seismic changes and the GPS respond when a loading is applied. The long smoothing window helps to extract the common long-term regional behavior of the vertical GPS components, filtering out the local response of each station. As would be expected, when the rainfall increases, the loading in the area increases, which generates a positive residual velocity variation, and at the same time, produces downward motion of the vertical position (Meier et al., 2010; Lecocq et al., 2017). This is consistent with regional observations made by Silverii et al. (2016), where they reported correlation between the vertical GPS data and the Gravity Recovery and Climate Experiment satellite observations.

This implies that the responses of the crust to the rain occur in two ways: in the first, the water generated by the rainfall accumulates in the aquifer, and as a result, it produces expansion of the area that is recorded by the horizontal GPS. This is a poroelastic reaction. In the second, the rainfall generates a load over the area that is measured by the vertical GPS motion. This is an elastic reaction. Although both of these mechanisms act simultaneously, they have peaks that are not in phase (see Figures 4c and 6c), and they are each measured with different intensities by the velocity variations of the seismic noise.

Finally, Figure 6 shows a highlighted period in which the pattern measured in the velocity variation does not match the seasonal loading. The most probable cause of this mismatch is the simultaneous high seismic activity in the area, including the M_W 5.0 earthquake, which occurs almost in the middle of the recorded anomaly in the velocity variation. All of this is coherent with the temporary velocity drop that dominates this period, which suggests stress release within the medium (Brenugier, Campillo, et al., 2008).

5 Conclusions

To disentangle the influence of the water content inside the crust from tectonic related events, we measured the variations in seismic velocity over 10 years in the Pollino region, Italy, for a single seismic station. These show yearly oscillations that are characteristic of seasonal factors and are superimposed over a multi-year pattern. As the water content in the soil is usually one of the main factors in the control of such velocity variations, we use here two models that estimate the water level inside an aquifer in the area, with the assumption that it is recharged by rainfall and that it loses water through two different mechanisms. Both of these models use constants where the values depend on the geometric particularities of the aquifer, which are unknown. Thus, we perform a grid search to compare the resulting water level models with the velocity variations, for different constants. This comparison recreates a modeled velocity variation that essentially modifies the overall amplitude and mean of the water level, to match those of the measured velocity variation, with the calculation of the root-mean-square error between the two models. Both of the models provide a good correlation with the velocity variations, showing that increase the levels of water in the aquifer decreases the velocity of the seismic waves. The increase in pore pressure as a consequence of the aquifer water leads to a reduction in the effective pressure in the medium, and therefore to a reduction in the seismic velocity. The models recreate the yearly seasonal behavior and the long multi-year trends. This shows that the total water inside the aquifer changes slowly, and is influenced by long-lasting periods of heavy rain or drought. The compar-

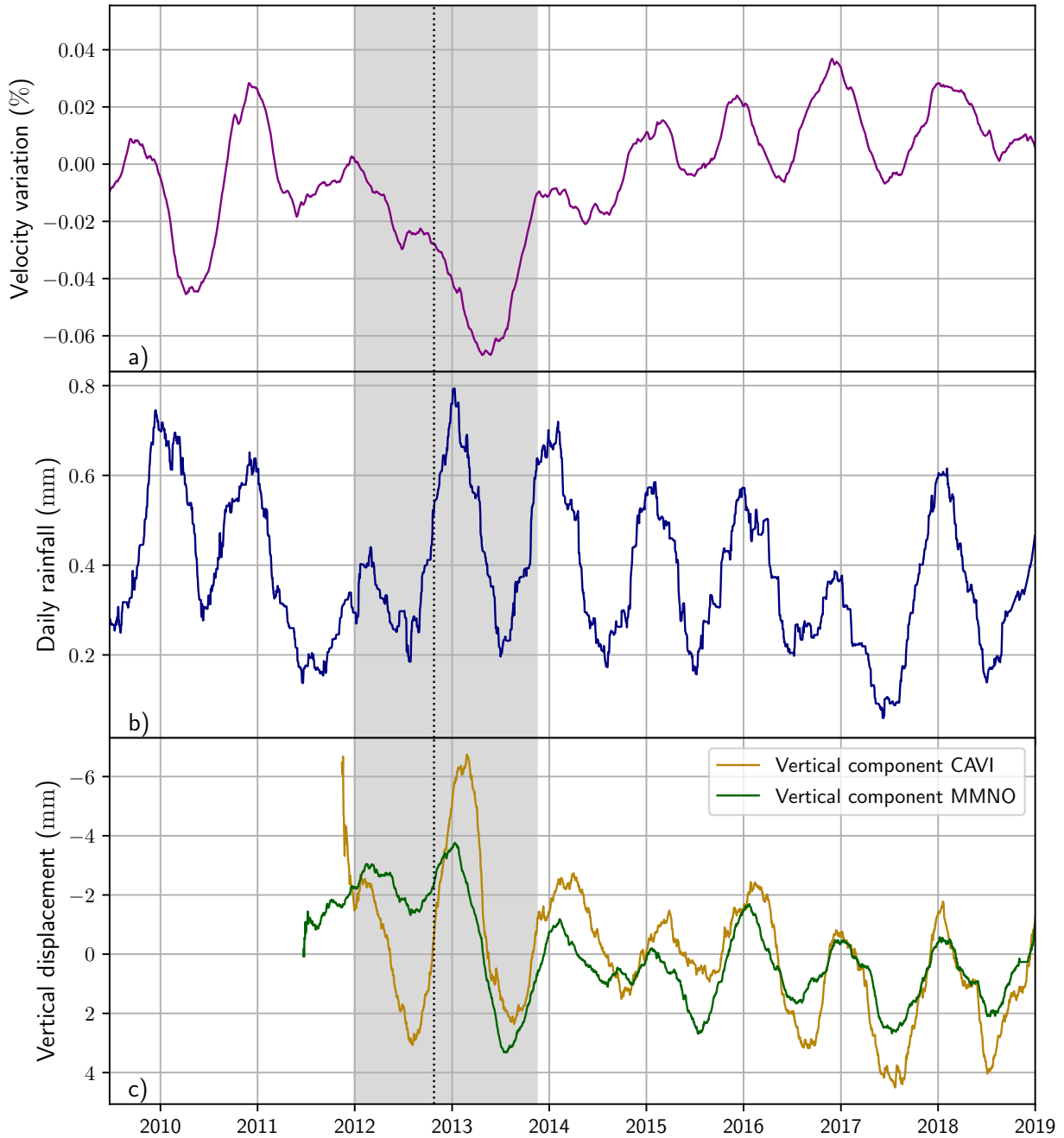


Figure 6. (a) Difference between the measured velocity variation in the seismic noise and the velocity variation of the water level model. (b) Rainfall. (c) Vertical GPS displacements of stations MMNO and CAVI (with the vertical axis inverted). The shading highlights the period for which the velocity variation is not explained by the water content of the soil, and is not in phase with the regional rainfall. The dashed line marks the date of the $M_W 5.0$ seismic event. All the plots are smoothed with a 180-day window

407 isons between the models and the measured $\delta v/v$ also show a systematic discrepancy be-
 408 tween them that lasts for 1 to 2 years, during which the seismic measurements show that
 409 the velocity on the area is lower than estimated by the model. This occurs in the same
 410 period as a $M_W 5.0$ earthquake, where slow slip events occur (Cheloni et al., 2017). This
 411 suggests that the velocity drop discrepancy is produced by stress release in the tectonic
 412 system through the seismic activity and the transient aseismic deformation. This dif-
 413 ference disappears by the end of 2013.

414 The NS component of the relative displacement between the VIGG and MMNO
 415 GPS stations across the fault suggests that the deformation in this area occurs synchronously
 416 with both the $\delta v/v$ and the water level of the aquifer for the period after the seismic ac-
 417 tivity that occurred between 2012 and 2013. The relative displacement in the $N36W$ di-
 418 rection follows the same behavior as both the measured and modeled velocity variations
 419 for the whole period that was recorded with GPS. This can be explained by the open-
 420 ing and closing of the fractures of the porous media under the pressure generated by the
 421 water, which generates the overall displacements recorded by the GPS. This behavior
 422 is also seen between all the other station pairs that are located in the study area. It also
 423 confirms our assumption of a poroelastic recharge and discharge process of the aquifer,
 424 upon which we base the water level models. The angle at which this occurs for the sta-
 425 tion pairs that include the MMNO station is always around 36° , which is close to the
 426 angle of the strike fault of the $M_W 5.0$ event (24°), possibly because for this direction the
 427 sharp displacement generated by the earthquake is minimized. Moreover, the angles that
 428 maximize this expansion-contraction mechanism for the station pairs that are not close
 429 to the earthquake (*i.e.*, VIGG-CAVI, VIGG-SALB, CAVI-SALB) show interesting dif-
 430 ferences that appear to be related to the shape of the aquifer or to local anisotropic be-
 431 havior.

432 Subtraction of the modeled velocity variations generated by the water level inside
 433 the aquifer from the observed seismic velocity variations reveals a pattern of weaker am-
 434 plitude that is in phase with the regional rainfall. The vertical displacements of the GPS
 435 in the study area are also closely negatively correlated with the rainfall. This indicates
 436 an elastic behavior of the area that occurs in parallel with the described poroelastic dy-
 437 namics. Thus, the rainfall generates a loading over the surface that results in subsidence
 438 of the elevation of the area (and therefore the negative correlation with the vertical GPS),
 439 and in a small increase in the stress of the crust (and therefore an increase in the seis-
 440 mic velocity), which are reflected in the $\delta v/v$.

441 Finally, this procedure highlights a period in which an anomalous velocity drop breaks
 442 the in-phase behavior between the residual seismic velocity and both the rainfall and the
 443 vertical GPS. This occurs simultaneously with a period of high seismic activity of the
 444 area, which includes a $M_W 5.0$ earthquake. Therefore, the velocity drop appears to be
 445 related to the stress release associated with the seismic activity of the area. This means
 446 that our analysis allows us to extract the seismic signature of the tectonic stress release
 447 despite two environment processes, *i.e.*, the elastic and poroelastic responses to the pre-
 448 cipitation, that occur simultaneously and dominate the variations in the seismic veloc-
 449 ity.

450 Acknowledgments

451 ERC F-image - This project has received funding from the European Research Coun-
 452 cil (ERC) under the European Union Horizon H2020 Research and Innovation program
 453 (grant agreement No 742335). The authors wish to thank Qing-Yu Wang and Francesco
 454 Fiorillo for the insightful discussions, and the constructive comments from the anony-
 455 mous reviewers. The seismic data can be downloaded at Istituto Nazionale di Geofisica
 456 e Vulcanologia (<https://doi.org/10.13127/SD/X0FXNH7QFY>). The RINEX daily files
 457 from RING GPS stations can be accessed at <http://ring.gm.ingv.it>. The rain data were
 458 provided by the Centro Funzionale Multirischi of the Calabria region (<http://www.cfd.calabria.it/>).

459 **References**

- 460 Akasaka, C., & Nakanishi, S. (2000). Correction of background gravity changes due
461 to precipitation: Oguni geothermal field, Japan. In *Proceedings world geother-
462 mal congress* (pp. 2471–2475).
- 463 Amoruso, A., Crescentini, L., Martino, S., Petitta, M., & Tallini, M. (2014). Cor-
464 relation between groundwater flow and deformation in the fractured car-
465 bonate Gran Sasso aquifer (INFN underground laboratories, central Italy).
466 *Water Resources Research*, *50*(6), 4858–4876. Retrieved from [https://
467 agupubs.onlinelibrary.wiley.com/doi/abs/10.1002/2013WR014491](https://agupubs.onlinelibrary.wiley.com/doi/abs/10.1002/2013WR014491) doi:
468 <https://doi.org/10.1002/2013WR014491>
- 469 Amos, C. B., Audet, P., Hammond, W. C., Bürgmann, R., Johanson, I. A., &
470 Blewitt, G. (2014). Uplift and seismicity driven by groundwater depletion
471 in central California. *Nature*, *509*(7501), 483–486. Retrieved from
472 <https://doi.org/10.1038/nature13275> doi: 10.1038/nature13275
- 473 Argus, D. F., Fu, Y., & Landerer, F. W. (2014). Seasonal variation in total water
474 storage in California inferred from GPS observations of vertical land motion.
475 *Geophysical Research Letters*, *41*(6), 1971–1980. Retrieved from [https://
476 agupubs.onlinelibrary.wiley.com/doi/abs/10.1002/2014GL059570](https://agupubs.onlinelibrary.wiley.com/doi/abs/10.1002/2014GL059570) doi:
477 10.1002/2014GL059570
- 478 ARPACAL. (n.d.). *Centro funzionale multirischi della Calabria*.
479 <http://www.cfd.calabria.it/>. Retrieved from <http://www.cfd.calabria.it/>
- 480 Bawden, G. W., Thatcher, W., Stein, R. S., Hudnut, K. W., & Peltzer, G. (2001).
481 Tectonic contraction across Los Angeles after removal of groundwater pump-
482 ing effects. *Nature*, *412*(6849), 812–815. Retrieved from [https://doi.org/
483 10.1038/35090558](https://doi.org/10.1038/35090558) doi: 10.1038/35090558
- 484 Borsa, A. A., Agnew, D. C., & Cayan, D. R. (2014). Ongoing drought-induced uplift
485 in the western United States. *Science*, *345*(6204), 1587–1590. Retrieved from
486 <https://science.sciencemag.org/content/345/6204/1587> doi: 10.1126/
487 science.1260279
- 488 Brenguier, F., Campillo, M., Hadziioannou, C., Shapiro, N. M., Nadeau, R. M., &
489 Larose, E. (2008). Postseismic Relaxation Along the San Andreas Fault at
490 Parkfield from Continuous Seismological Observations. *Science*, *321*(5895),
491 1478 LP – 1481. Retrieved from [http://science.sciencemag.org/content/
492 321/5895/1478.abstract](http://science.sciencemag.org/content/321/5895/1478.abstract) doi: 10.1126/science.1160943
- 493 Brenguier, F., Shapiro, N. M., Campillo, M., Ferrazzini, V., Duputel, Z., Coutant,
494 O., & Nercessian, A. (2008). Towards forecasting volcanic eruptions us-
495 ing seismic noise. *Nature Geoscience*, *1*(2), 126–130. Retrieved from
496 <https://doi.org/10.1038/ngeo104> doi: 10.1038/ngeo104
- 497 Campillo, M. (2006). Phase and Correlation in ‘Random’ Seismic Fields and the Re-
498 construction of the Green Function. *pure and applied geophysics*, *163*(2), 475–
499 502. Retrieved from <https://doi.org/10.1007/s00024-005-0032-8> doi: 10.
500 .1007/s00024-005-0032-8
- 501 Campillo, M., & Paul, A. (2003). Long-Range Correlations in the Diffuse Seismic
502 Coda. *Science (New York, N.Y.)*, *299*, 547–549. doi: 10.1126/science.1078551
- 503 Chanard, K., Avouac, J. P., Ramillien, G., & Genrich, J. (2014). Modeling de-
504 formation induced by seasonal variations of continental water in the Hi-
505 malaya region: Sensitivity to Earth elastic structure. *Journal of Geophys-
506 ical Research: Solid Earth*, *119*(6), 5097–5113. Retrieved from [https://
507 agupubs.onlinelibrary.wiley.com/doi/abs/10.1002/2013JB010451](https://agupubs.onlinelibrary.wiley.com/doi/abs/10.1002/2013JB010451) doi:
508 10.1002/2013JB010451
- 509 Chaussard, E., Bürgmann, R., Shirzaei, M., Fielding, E. J., & Baker, B. (2014).
510 Predictability of hydraulic head changes and characterization of aquifer-system
511 and fault properties from insar-derived ground deformation. *Journal of Geo-
512 physical Research: Solid Earth*, *119*(8), 6572–6590.
- 513 Cheloni, D., D’Agostino, N., Selvaggi, G., Avallone, A., Fornaro, G., Giuliani,

- 514 R., ... Tizzani, P. (2017). Aseismic transient during the 2010-2014 seis-
515 mic swarm: evidence for longer recurrence of $M_i \neq 6.5$ earthquakes in
516 the Pollino gap (Southern Italy)? *Scientific reports*, 7(1), 576. doi:
517 10.1038/s41598-017-00649-z
- 518 Clements, T., & Denolle, M. A. (2018). Tracking groundwater levels using the
519 ambient seismic field. *Geophysical Research Letters*, 45(13), 6459-6465.
520 Retrieved from [https://agupubs.onlinelibrary.wiley.com/doi/abs/](https://agupubs.onlinelibrary.wiley.com/doi/abs/10.1029/2018GL077706)
521 10.1029/2018GL077706 doi: <https://doi.org/10.1029/2018GL077706>
- 522 D'Agostino, N., Silverii, F., Amoroso, O., Convertito, V., Fiorillo, F., Ventafridda,
523 G., & Zollo, A. (2018). Crustal Deformation and Seismicity Modulated by
524 Groundwater Recharge of Karst Aquifers. *Geophysical Research Letters*,
525 45(22), 12,212–253,262. Retrieved from [https://agupubs.onlinelibrary](https://agupubs.onlinelibrary.wiley.com/doi/abs/10.1029/2018GL079794)
526 [.wiley.com/doi/abs/10.1029/2018GL079794](https://agupubs.onlinelibrary.wiley.com/doi/abs/10.1029/2018GL079794) doi: 10.1029/2018GL079794
- 527 Daniele, T., Braitenberg, C., & Nagy, I. (2012). Karst deformations due to envi-
528 ronmental factors: Evidences from the horizontal pendulums of Grotta Gi-
529 gante, Italy. *Bollettino di Geofisica Teorica ed Applicata*, 53, 331–345. doi:
530 10.4430/bgta0049
- 531 Fiorillo, F. (2011). Tank-reservoir drainage as a simulation of the recession limb of
532 karst spring hydrographs. *Hydrogeology Journal*, 19, 1009–1019. doi: 10.1007/
533 s10040-011-0737-y
- 534 Galloway, D., & Burbey, T. (2011). Review: Regional land subsidence accompanying
535 groundwater extraction. *Hydrogeology Journal - HYDROGEOL J*, 19. doi: 10
536 .1007/s10040-011-0775-5
- 537 Hillers, G., Campillo, M., Brenguier, F., Moreau, L., Agnew, D. C., & Ben-Zion,
538 Y. (2019). Seismic Velocity Change Patterns Along the San Jacinto Fault
539 Zone Following the 2010 M7.2 El Mayor-Cucapah and M5.4 Collins Valley
540 Earthquakes. *Journal of Geophysical Research: Solid Earth*, 124(7), 7171–
541 7192. Retrieved from [https://agupubs.onlinelibrary.wiley.com/doi/abs/](https://agupubs.onlinelibrary.wiley.com/doi/abs/10.1029/2018JB017143)
542 10.1029/2018JB017143 doi: 10.1029/2018JB017143
- 543 Hillers, G., Campillo, M., & Ma, K.-F. (2014). Seismic velocity variations at TCDP
544 are controlled by MJO driven precipitation pattern and high fluid discharge
545 properties. *Earth and Planetary Science Letters*, 391, 121–127. Retrieved from
546 <http://www.sciencedirect.com/science/article/pii/S0012821X14000569>
547 doi: <https://doi.org/10.1016/j.epsl.2014.01.040>
- 548 INGV Seismological Data Centre. (2006). *Italian National Seismic Network*. Istito
549 Nazionale di Geofisica e Vulcanologia (INGV), Italy. doi: [https://doi.org/](https://doi.org/10.13127/SD/X0FXnH7QfY)
550 10.13127/SD/X0FXnH7QfY
- 551 Istituto Nazionale di Geofisica e Vulcanologia INGV. (2016). *Rete integrata*
552 *nazionale gps (ring)*. Istituto Nazionale di Geofisica e Vulcanologia INGV.
553 Retrieved from <http://ring.gm.ingv.it/> doi: 10.13127/RING
- 554 King, N. E., Argus, D., Langbein, J., Agnew, D. C., Bawden, G., Dollar, R. S., ...
555 Barseghian, D. (2007). Space geodetic observation of expansion of the San
556 Gabriel Valley, California, aquifer system, during heavy rainfall in winter 2004
557 2005. *Journal of Geophysical Research: Solid Earth*, 112(B3). Retrieved
558 from [https://agupubs.onlinelibrary.wiley.com/doi/abs/10.1029/](https://agupubs.onlinelibrary.wiley.com/doi/abs/10.1029/2006JB004448)
559 2006JB004448 doi: 10.1029/2006JB004448
- 560 Lecocq, T., Longuevergne, L., Pedersen, H. A., Brenguier, F., & Stammer, K.
561 (2017). Monitoring ground water storage at mesoscale using seismic noise:
562 30 years of continuous observation and thermo-elastic and hydrological mod-
563 eling. *Scientific Reports*, 7(1), 14241. Retrieved from [https://doi.org/](https://doi.org/10.1038/s41598-017-14468-9)
564 10.1038/s41598-017-14468-9 doi: 10.1038/s41598-017-14468-9
- 565 Meier, U., Shapiro, N. M., & Brenguier, F. (2010). Detecting seasonal variations
566 in seismic velocities within Los Angeles basin from correlations of ambient
567 seismic noise. *Geophysical Journal International*, 181(2), 985–996. Re-
568 trieved from <https://doi.org/10.1111/j.1365-246X.2010.04550.x> doi:

- 569 10.1111/j.1365-246X.2010.04550.x
- 570 Michetti, A. M., Ferreli, L., Esposito, E., Porfido, S., Blumetti, A. M., Vittori, E.,
571 ... Roberts, G. P. (2000, 01). Ground Effects during the 9 September 1998,
572 Mw = 5.6 Lauria Earthquake and the Seismic Potential of the “Aseismic”
573 Pollino Region in Southern Italy. *Seismological Research Letters*, 71(1),
574 31-46. Retrieved from <https://doi.org/10.1785/gssrl.71.1.31> doi:
575 10.1785/gssrl.71.1.31
- 576 Nof, R., Ziv, A., Doin, M.-P., Baer, G., Fialko, Y., Wdowinski, S., ... Bock, Y.
577 (2012). Rising of the lowest place on Earth due to Dead Sea water-level drop:
578 Evidence from SAR interferometry and GPS. *Journal of Geophysical Research*
579 (*Solid Earth*), 117, 5412–. doi: 10.1029/2011JB008961
- 580 Ojha, C., Werth, S., & Shirzaei, M. (2019). Groundwater loss and aquifer system
581 compaction in san joaquin valley during 2012–2015 drought. *Journal of Geo-*
582 *physical Research: Solid Earth*, 124(3), 3127–3143.
- 583 Papanikolaou, I. D., & Roberts, G. P. (2007). Geometry, kinematics and defor-
584 mation rates along the active normal fault system in the southern apennines:
585 Implications for fault growth. *Journal of Structural Geology*, 29(1), 166–188.
- 586 Parotidis, M., Rothert, E., & Shapiro, S. A. (2003). Pore-pressure diffusion: A pos-
587 sible triggering mechanism for the earthquake swarms 2000 in Vogtland/NW-
588 Bohemia, central Europe. *Geophysical Research Letters*, 30(20). Retrieved
589 from [https://agupubs.onlinelibrary.wiley.com/doi/abs/10.1029/](https://agupubs.onlinelibrary.wiley.com/doi/abs/10.1029/2003GL018110)
590 [2003GL018110](https://agupubs.onlinelibrary.wiley.com/doi/abs/10.1029/2003GL018110) doi: 10.1029/2003GL018110
- 591 Passarelli, L., Hainzl, S., Cesca, S., Maccaferri, F., Mucciarelli, M., Roessler, D.,
592 ... Rivalta, E. (2015). Aseismic transient driving the swarm-like seismic se-
593 quence in the Pollino range, Southern Italy. *Geophysical Journal International*,
594 201(3), 1553–1567. Retrieved from [http://academic.oup.com/gji/article/](http://academic.oup.com/gji/article/201/3/1553/776740/Aseismic-transient-driving-the-swarmlike-seismic)
595 [201/3/1553/776740/Aseismic-transient-driving-the-swarmlike-seismic](http://academic.oup.com/gji/article/201/3/1553/776740/Aseismic-transient-driving-the-swarmlike-seismic)
596 doi: 10.1093/gji/ggv111
- 597 Peng, Z., & Gomberg, J. (2010). An integrated perspective of the contin-
598 uum between earthquakes and slow-slip phenomena. *Nature Geoscience*,
599 3(9), 599–607. Retrieved from <https://doi.org/10.1038/ngeo940> doi:
600 10.1038/ngeo940
- 601 Poli, P., Marguin, V., Wang, Q., D’Agostino, N., & Johnson, P. (2020). Seasonal
602 and Coseismic Velocity Variation in the Region of L’Aquila From Single Sta-
603 tion Measurements and Implications for Crustal Rheology. *Journal of Geophys-*
604 *ical Research: Solid Earth*, 125(7), e2019JB019316. Retrieved from [https://](https://agupubs.onlinelibrary.wiley.com/doi/abs/10.1029/2019JB019316)
605 agupubs.onlinelibrary.wiley.com/doi/abs/10.1029/2019JB019316 doi:
606 10.1029/2019JB019316
- 607 Poupinet, G., Ellsworth, W. L., & Frechet, J. (1984). Monitoring velocity varia-
608 tions in the crust using earthquake doublets: An application to the Calaveras
609 Fault, California. *Journal of Geophysical Research: Solid Earth*, 89(B7), 5719–
610 5731. Retrieved from [https://agupubs.onlinelibrary.wiley.com/doi/abs/](https://agupubs.onlinelibrary.wiley.com/doi/abs/10.1029/JB089iB07p05719)
611 [10.1029/JB089iB07p05719](https://agupubs.onlinelibrary.wiley.com/doi/abs/10.1029/JB089iB07p05719) doi: 10.1029/JB089iB07p05719
- 612 Rivet, D., Brenguier, F., & Cappa, F. (2015). Improved detection of preerup-
613 tive seismic velocity drops at the Piton de La Fournaise volcano. *Geo-*
614 *physical Research Letters*, 42(15), 6332–6339. Retrieved from [https://](https://agupubs.onlinelibrary.wiley.com/doi/abs/10.1002/2015GL064835)
615 agupubs.onlinelibrary.wiley.com/doi/abs/10.1002/2015GL064835 doi:
616 10.1002/2015GL064835
- 617 Sens-Schönfelder, C., & Wegler, U. (2006). Passive image interferometry and sea-
618 sonal variations of seismic velocities at Merapi Volcano, Indonesia. *Geophysical*
619 *Research Letters*, 33(21). Retrieved from [https://agupubs.onlinelibrary](https://agupubs.onlinelibrary.wiley.com/doi/abs/10.1029/2006GL027797)
620 [.wiley.com/doi/abs/10.1029/2006GL027797](https://agupubs.onlinelibrary.wiley.com/doi/abs/10.1029/2006GL027797) doi: 10.1029/2006GL027797
- 621 Seydoux, L., de Rosny, J., & Shapiro, N. M. (2017). Pre-processing ambient noise
622 cross-correlations with equalizing the covariance matrix eigenspectrum. *Geo-*
623 *physical Journal International*, 210(3), 1432–1449. doi: 10.1093/gji/ggx250

- 624 Shapiro, N. M., & Campillo, M. (2004). Emergence of broadband Rayleigh waves
625 from correlations of the ambient seismic noise. *Geophysical Research Letters*,
626 *31*(7). Retrieved from [https://agupubs.onlinelibrary.wiley.com/doi/](https://agupubs.onlinelibrary.wiley.com/doi/abs/10.1029/2004GL019491)
627 [abs/10.1029/2004GL019491](https://agupubs.onlinelibrary.wiley.com/doi/abs/10.1029/2004GL019491) doi: 10.1029/2004GL019491
- 628 Silverii, F., D'Agostino, N., Métois, M., Fiorillo, F., & Ventafridda, G. (2016). Tran-
629 sient deformation of karst aquifers due to seasonal and multiyear groundwater
630 variations observed by GPS in southern Apennines (Italy). *Journal of Geo-*
631 *physical Research: Solid Earth*, *121*(11), 8315–8337. Retrieved from [https://](https://agupubs.onlinelibrary.wiley.com/doi/abs/10.1002/2016JB013361)
632 agupubs.onlinelibrary.wiley.com/doi/abs/10.1002/2016JB013361 doi:
633 10.1002/2016JB013361
- 634 Tsai, V. C. (2011). A model for seasonal changes in GPS positions and seis-
635 mic wave speeds due to thermoelastic and hydrologic variations. *Journal*
636 *of Geophysical Research: Solid Earth*, *116*(B4). Retrieved from [https://](https://agupubs.onlinelibrary.wiley.com/doi/abs/10.1029/2010JB008156)
637 agupubs.onlinelibrary.wiley.com/doi/abs/10.1029/2010JB008156 doi:
638 10.1029/2010JB008156
- 639 Wang, Q. Y., Brenguier, F., Campillo, M., Lecointre, A., Takeda, T., & Aoki, Y.
640 (2017). Seasonal Crustal Seismic Velocity Changes Throughout Japan.
641 *Journal of Geophysical Research: Solid Earth*, *122*(10), 7987–8002. doi:
642 10.1002/2017JB014307
- 643 Watson, K. M., Bock, Y., & Sandwell, D. T. (2002). Satellite interferometric obser-
644 vations of displacements associated with seasonal groundwater in the Los An-
645 geles basin. *Journal of Geophysical Research: Solid Earth*, *107*(B4), ETG 8–
646 1–ETG 8–15. Retrieved from [https://agupubs.onlinelibrary.wiley.com/](https://agupubs.onlinelibrary.wiley.com/doi/abs/10.1029/2001JB000470)
647 [doi/abs/10.1029/2001JB000470](https://agupubs.onlinelibrary.wiley.com/doi/abs/10.1029/2001JB000470) doi: 10.1029/2001JB000470